



1 A time series analysis of transparent exopolymer particle distributions and C:N
2 stoichiometry in the subtropical North Pacific: a key process in net community
3 production and preformed nitrate anomalies?
4

5 Kieran Curran¹, Tracy Villareal², Robert T. Letscher^{1,3}

6 1 Ocean Process Analysis Laboratory, University of New Hampshire, Durham, NH, 03824 USA

7 2 Marine Science Institute, University of Texas at Austin, Port Aransas, TX 78373 USA

8 3 Department of Earth Sciences, University of New Hampshire, Durham, NH 03824 USA

9 Correspondence to: Robert T. Letscher (robert.letscher@unh.edu)

10 Abstract

11 Within the oligotrophic subtropical oceans, summertime DIC drawdown despite nutrient limitation in
12 surface waters and subsurface oxygen consumption in the absence of Redfieldian stoichiometric nitrate
13 release are two phenomena still awaiting a full mechanistic characterization. The distribution, intensity
14 and seasonality of these phenomena are identified with preformed nitrate as a tracer, where negative
15 preformed nitrate (NPN) anomalies below the euphotic zone correspond to oxygen consumption without
16 Redfieldian NO_3^- release, and positive preformed nitrate (PPN) anomalies found within the upper 100m
17 occur where O_2 is produced without stoichiometric NO_3^- drawdown. Many processes that may contribute
18 to these anomalies including N_2 fixation, non-Redfieldian DOM cycling, vertically migrating phytoplankton,
19 heterotrophic NO_3^- uptake and vertical NO_3^- injection events have been measured or modelled, yet
20 generally cannot fully account for the magnitudes of preformed nitrate anomalies and excess DIC
21 drawdown observed in many oligotrophic subtropical waters. One other candidate process that may
22 contribute to both phenomena is the formation of carbon-rich transparent exopolymer particles (TEP) and
23 Coomassie-stainable particles (CSP) from dissolved organic precursors in surface waters and their
24 subsequent remineralization below the subsurface chlorophyll maximum (SCM). However, few data exist
25 to quantify exopolymer production and vertical distributions in oligotrophic oceans over an annual cycle,
26 which is necessary to understand their potential role in the evolution of seasonal preformed nitrate
27 anomalies and DIC drawdown.

28 To investigate the significance of exopolymer formation and export to North Pacific subtropical gyre
29 biogeochemistry, we undertook a multi-year time-series (Jan 2020 – Sep 2022) analysis of TEP, CSP and
30 total dissolved polysaccharides concentrations at Station ALOHA ($22^\circ 45', 158^\circ \text{W}$), and along a transect
31 from $22^\circ 45'$ to 31°N to measure latitudinal variability in June 2021. Exopolymer C:N stoichiometry at
32 Station ALOHA varied between 16.4 – 34.3, with values being more carbon-rich in summer; ratios were
33 higher (32-38) toward the gyre centre at 31°N . TEP concentrations were consistently elevated in surface
34 waters through Spring-Autumn (4-8 $\mu\text{M C}$ after carbon conversion) at Station ALOHA with lower
35 concentrations ($\sim 1.5\text{-}3 \mu\text{M C}$) and more uniform vertical distribution during winter, indicating that TEP
36 accumulated in surface waters may vertically sink and be exported with winter mixing. The accumulation
37 of TEP in surface waters through Spring-Autumn and its subsequent export may account for 6.5-20% of
38 net community production (NCP), helping reduce the estimated imbalance of N supply and N demand at
39 this site to $<10\%$. The upper ocean TEP cycle may explain 22-67% of the observed PPN/NPN anomalies,
40 helping to close the C, N, and O_2 budgets at station ALOHA, while leaving room for significant contributions



41 from other processes such as vertically migrating phytoplankton and heterotrophic nitrate uptake to be
42 further validated. These results suggest that exopolymer production and cycling may be more important
43 to open ocean carbon biogeochemistry than previously expected, with considerable seasonality and
44 spatial variability influenced by physical processes and phytoplankton activity.

45



46 1 Introduction

47

48 Subtropical oceans constitute one of earth's largest biomes, where the euphotic water column exhibits
49 sustained macronutrient limitation due to strong thermal stratification (Reygondeau et al., 2013).
50 Consistently low euphotic zone chlorophyll concentrations observed in these regions lead to depressed
51 primary production estimates using ocean-colour satellite and bio-optical float profile data (Longhurst et
52 al., 1995; Long et al., 2021; Westberry et al., 2023). Despite this assumption of low productivity, various
53 measured rates of annual net community production (NCP) and total annual carbon export from the ocean
54 subtropics suggest a biological pump strength that is maintained at levels consistent with other
55 mesotrophic oceanic regions (Gruber et al., 1998; Emerson, 2014; Teng et al., 2014; Roshan and DeVries,
56 2017; Quay et al., 2020; Karl et al., 2021).

57 Moderate rates of summertime surface dissolved inorganic carbon (DIC) drawdown are observed in low-
58 chlorophyll Atlantic and Pacific subtropical oceans ($2\text{-}3 \text{ mol C m}^{-2} \text{ y}^{-1}$) despite limiting nitrate and
59 phosphate concentrations, and stratification that would seem to limit diapycnal supply of nutrients to the
60 euphotic zone for most of the year (Sambrotto et al., 1993; Michaels et al., 1994; Dave and Lozier, 2010;
61 Williams et al., 2013; Emerson, 2014). Processes of nutrient enrichment such as N_2 fixation, episodic
62 mixing events, and iron-rich dust deposition are unable to fully account for sufficient nutrient supply to
63 sustain this persistent summertime anomaly (Johnson et al., 2010; Chow et al., 2017; Fawcett et al., 2018;
64 Letscher and Villareal, 2018; Letelier et al., 2019; Karl et al., 2021). In addition, most subtropical regions
65 exhibit respiration without concomitant nitrate release expected from the remineralization of Redfieldian
66 organic matter, producing a widespread negative preformed nitrate (preNO_3^-) anomaly between $\sim 120\text{-}$
67 180m (Emerson and Hayward, 1995; Abell et al., 2005; Ascani et al., 2013; Letscher and Villareal, 2018;
68 Smyth and Letscher, 2023). The introduction of allochthonous macronutrient supply to the surface mixed
69 layer (SML) or the production and export of non-Redfieldian organic matter (high elemental
70 carbon:nitrogen ratio) within the SML are two potential processes which may couple these two
71 phenomena and help explain the elevated surface DIC drawdown and negative preNO_3^- below the sub-
72 surface chlorophyll maximum (SCM) in these regions.

73 Transparent exopolymer particles (TEP), mostly comprised of acidic polysaccharides, are ubiquitous
74 throughout the oceans, where they tend to accumulate in surface waters due to their low density (Azetsu-
75 Scott and Passow, 2004). Exopolymers are typically observed as being carbon-rich, with C:N ratios of $>20:1$
76 (Mari et al., 2001; Engel and Passow, 2001; Passow, 2002b; Guo et al., 2022), which makes them a
77 candidate for SML DIC drawdown with minimal nitrogen requirement, particularly if composed of pure
78 carbohydrate (e.g. $1 \text{ C} : 1 \text{ O}_2 : 0 \text{ N}$). While most abundant during large blooms of phytoplankton in
79 eutrophic waters, TEP and their precursors are produced by a wide variety of phytoplankton and bacteria
80 across different marine and aquatic environments (Passow et al., 1994; Nosaka et al., 2017; Zamanillo et
81 al., 2019). Sinking exopolymer aggregates constitute a significant flux of POC to the upper mesopelagic
82 zone, where much of this organic matter may be consumed by aggregate-associated bacteria (Wurl et al.,
83 2011b; Nagata et al., 2021) and sometimes zooplankton (Ling and Alldredge, 2003).

84 TEP production from phytoplankton exudates is associated with excess DIC drawdown even in nutrient-
85 replete waters, with carbon overconsumption as high as 30-40% with respect to nitrate and phosphate
86 removal and POM C:N:P stoichiometry (Toggweiler, 1993). In addition to excess DIC consumption, SML
87 exopolymer production may increase as cells are stressed by nutrient limitation or photo-oxidative stress



88 (Berman-Frank et al., 2007; Ortega-Retuerta et al., 2009a; Iuculano et al., 2017), both conditions being
89 persistent in many subtropical surface waters. Therefore, despite low microbial biomass in these
90 oligotrophic regions, significant TEP production and seasonal variability may still occur.

91 Given that different oligotrophic regions exhibit significant variability in the elemental stoichiometry of
92 organic matter including biomass (Martiny et al., 2013), detrital POM, and DOM (Letscher and Moore,
93 2015; Liang et al., 2023), across depth and time, region-specific measurements are needed to quantify the
94 importance of exopolymer particles to pelagic biogeochemistry of different regions (McCarthy et al., 1996;
95 Mari et al., 2001; Passow, 2002b; Beauvais et al., 2003). In this study, we aim to assess whether significant
96 depth, temporal, and latitudinal gradients exist in exopolymer abundance and its associated C:N content
97 that may help to explain the excess DIC drawdown/observed productivity and seasonal subsurface
98 preNO_3^- anomalies in the subtropical oceans. Over three years we collected measurements in the North
99 Pacific Subtropical Gyre (NPSG) of two classes of exopolymers: carbohydrate-rich transparent exopolymer
100 particles (TEP) and protein-containing Coomassie-stainable particles (CSP) in addition to dissolved
101 carbohydrate concentrations, which are precursor molecules of larger exopolymer particles (Passow,
102 2000; Ortega-Retuerta et al., 2009b; Arnosti et al., 2021), to quantify their concentrations, vertical
103 distributions, and seasonal and latitudinal variability. In order to produce quantitative estimates of TEP
104 and CSP concentrations we also directly estimated the organic C and N content of exopolymers
105 spontaneously assembled under controlled conditions in the field to convert TEP and CSP values to carbon
106 and nitrogen equivalents. With these quantitative estimates of TEP-C and CSP-N concentrations, we then
107 discuss the significance of exopolymers and dissolved carbohydrates to overall organic carbon
108 biogeochemistry in the study region and subtropical oceans more generally.

109

110

111

112

113

114

115

116

117

118

119

120

121

122



123 2 Methods

124 2.1 Sample collection

125 Water samples for measurements of TEP, CSP, and dissolved polysaccharides were collected using a
126 Niskin rosette onboard the RV *Kilo Moana* from 15 cruises between January 2020 and September 2022.
127 14 cruises were part of the Hawaiian Ocean Time-series (HOT) sampling program at Station ALOHA (22°
128 45' N 158° W), with 1 cruise sampling 10 stations in the North Pacific Gyre along a nominal 158°W
129 transect from Station ALOHA to 31° N during June 2021, also on RV *Kilo Moana* (Fig. 1). Vertical profiles
130 of salinity (Sea-Bird SBE-09), temperature (Sea-Bird SBE-3 Plus) and oxygen (Sea-Bird SBE-43) were also
131 collected from the rosette CTD instrument package.

132

133

134

135

136

137

138

139

140

141

142

143

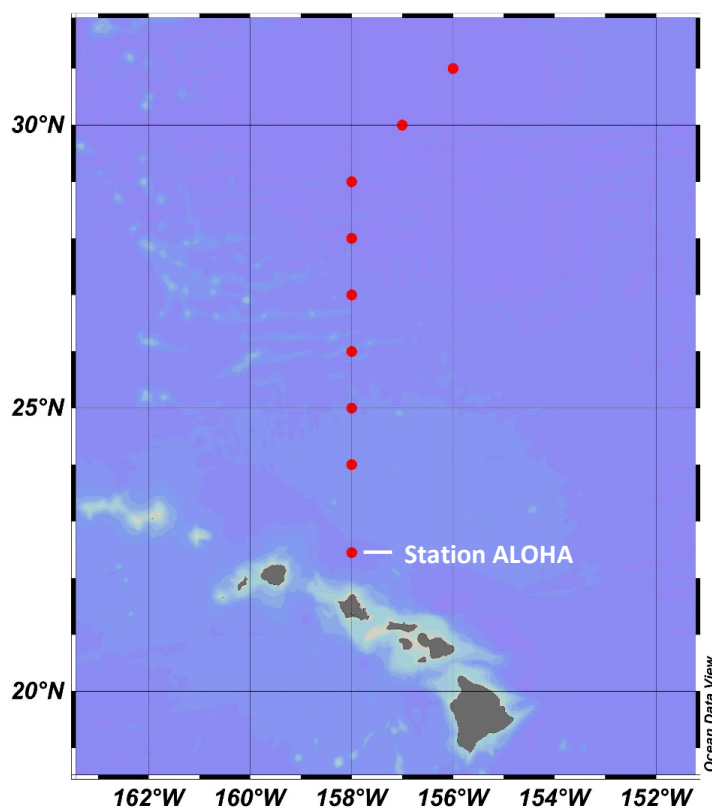
144

145

146

147

148



149 Figure 1. Map showing the location of Station ALOHA where time series measurements were collected and the
150 stations along the June 2021 transect between ALOHA and 31°N.

151 2.2 Quantification of transparent exopolymer particles (TEP) and Coomassie-stainable 152 particles (CSP)

153 Water samples for TEP and CSP (0.5-2.0L) were taken from 5-8 depths and stored in polycarbonate bottles
154 (Corning) in blacked-out carriers until filtration. Samples were processed from deepest to shallowest to
155 minimize any effects of small temperature changes on exopolymer formation dynamics. Water samples



156 for TEP and CSP were filtered using 0.4 μm pore-size, 25mm diameter polycarbonate filters (Whatman)
157 using a peristaltic pump (Masterflex). Filters were then placed onto a vacuum filtration rig and dyed with
158 acidified (pH 2.5) 0.02% Alcian Blue (AB) solution (Alcian Blue 8X, Sigma Aldrich) for TEP samples following
159 Bittar et al. (2015) and 0.04% Coomassie brilliant blue (CBB) (SERVA) solution (pH 7.4) for CSP samples
160 following Cisternas-Novoa et al. (2014). Dyed filters were placed in polypropylene vials (Falcon) and frozen
161 at -20°C , and 2-day shipped back to the shore-based laboratory in ice-packed coolers (Pelican). TEP
162 samples were extracted in 6ml 80% sulphuric acid solution for 2 hrs and absorbance read at 787nm. CSP
163 samples were extracted in 4ml 3% sodium dodecyl sulphate (SDS) in 50% isopropyl alcohol solution for 2
164 hrs at 37°C under ultrasonication and read at 615nm. Absorbance values were blanked against the same
165 type of polycarbonate filters after filtration of 500ml ultrapure water. Blanks were also taken with 500ml
166 0.2 μm filtered seawater to check that there was no bias from sub-0.2 μm organic material from seawater
167 that could be retained on the filters. These blanks were not significantly different and had a combined
168 coefficient of variation of 0.039. Absorbance values were calibrated against a dilution series of xanthan
169 gum (Sigma) and bovine albumin (BA) (Sigma) for TEP and CSP respectively. Concentration units are
170 therefore expressed as $\mu\text{g C L}^{-1}$ in xanthan equivalents and $\mu\text{g N L}^{-1}$ in bovine albumin equivalents
171 preceding any subsequent conversions. TEP sample replicates had a mean coefficient of variation of 0.04
172 and CSP samples 0.14 ($n=24$) from 8 sets of triplicate measurements.

173 2.3 Dissolved carbohydrates

174 Water samples for dissolved carbohydrate analysis were gravity filtered from the Niskin rosette using a
175 47mm combusted GF/F filter (Whatman) (0.7 μm nominal pore size) into acid cleaned and furnace glass
176 vials. Vials were frozen at -20°C and transported similar to above for lab analysis. Using the approach of
177 Mykkestad et al (1997), total HCl-hydrolysable carbohydrates (TCHO) were measured against a glucose
178 calibration standard and expressed in μM carbon. The method uses the alkaline ferricyanide reaction with
179 2,4,6-tripyridyl-*s*-triazine (TPTZ) that produces a deep violet color with reduced iron, allowing sensitive
180 measurement of low carbohydrate concentrations with spectrophotometry. Reagents were made fresh
181 for each run of samples and kept in blacked-out glassware. Coefficients of variation ranged between 2.5%
182 for low concentrations ($<20 \mu\text{M}$) to 0.9% for high concentrations ($>30 \mu\text{M}$) of carbohydrate.

183 2.4 Carbon and Nitrogen conversion factors

184 During field sampling at station ALOHA (22.75°N , 158°W) and from 31°N , 156°W in June 2021 and October
185 2021 from station ALOHA alone, 3 x 10 litre volumes of seawater from two depths (5m, 125m) were
186 filtered through a 0.2 μm capsule filter (Pall) into opaque HDPE plastic bottles and stored in the dark while
187 at sea at sample depth temperature $\pm 1^{\circ}\text{C}$. Bottles were left for 80-100hrs to allow sufficient time for
188 exopolymer to spontaneously reform from the dissolved fraction. From these bottles, duplicate filtrations
189 (1.5L) were performed for TEP and CSP concentrations and duplicate filtrations for particulate carbon and
190 nitrogen were taken onto 47mm GF filters (Whatman) for CHN analysis of the collected exopolymer
191 particles.

192 Particulate carbon and nitrogen data were then used with the measurements of TEP and CSP to convert
193 xanthan and bovine albumin equivalents to $\mu\text{M C}$ and $\mu\text{M N}$ using carbon and nitrogen conversion factors
194 (CCF and NCF).

195

196



197 $Carbon\ conversion\ factor = \frac{\mu M\ Particulate\ Carbon}{\mu g\ Xanthan\ equiv\ L^{-1}}$ (1)

198 $Nitrogen\ conversion\ factor = \frac{\mu M\ Particulate\ Nitrogen}{\mu g\ BA\ equiv\ L^{-1}}$ (2)

199 TEP carbon (TEP-C) and CSP nitrogen (CSP-N) concentrations are thereafter converted and expressed in
200 μM units of carbon and nitrogen respectively.

201

202 3 Results & Discussion

203 3.1 Carbon and Nitrogen conversion factors

204 Table 1. CSP-N and TEP-C conversion factors and exopolymer C:N ratios measured from exopolymer ingrowth
205 incubations of 0.2 μm -filtered seawater conducted in June and October '21 at station ALOHA and at the northern
206 end of the June '21 transect (31°N, 156°W); values in parentheses are coefficients of variation.

Conversions	CSP-N Jun 21	CSP-N Oct 21	TEP-C Jun 21	TEP-C Oct 21	C:N Jun 21	C:N Oct 21
ALOHA 5 m	0.018 (0.03)	0.012 (0.18)	0.529 (0.02)	0.577 (0.02)	25.7 (0.01)	18.54 (0.16)
ALOHA 125 m	0.005 (0.23)	0.013 (0.27)	0.627 (0.05)	0.600 (0.19)	34.3 (0.11)	16.40 (0.36)
31°N 5m	0.004 (0.05)		0.656 (0.12)		33.2 (0.04)	
31°N 125m	0.003 (0.19)		0.759 (0.05)		38.1 (0.01)	

207

208 Carbon conversion factors for TEP-C at station ALOHA varied between 0.529-0.627 μM C per μg xanthan
209 equivalent L^{-1} with mean surface values being lower than at 125 m (Table 1). These values are consistent
210 with the frequently used conversion factor of 0.6 from Engel and Passow (2001). Nitrogen conversion
211 factors for CSP-N varied by a factor of ~6 between 0.003-0.018 with lower organic nitrogen content found
212 at 31°N than at station ALOHA (Table 1.). C:N ratio (16.4-34.3) at ALOHA varied more than carbon
213 conversion factors (0.529-0.627), e.g. by a factor of ~2 and ~1.2 respectively, with summertime samples
214 from 125 m being most carbon-rich and samples from October at 125 m having the lowest C:N ratios. All
215 samples were carbon-rich with respect to the canonical Redfield ratio, with exopolymer C:N ratios at
216 station ALOHA being significantly higher in summer than autumn at 5 m ($p=0.008$) and 125 m ($p=0.003$)
217 using one-factor ANOVA, consistent with the observations of (Michaels et al., 1994). Summertime C:N
218 ratios were higher in northern gyre-associated waters (31°N) than at station ALOHA, e.g. 33 – 38 vs. 26 –
219 34, however only significantly so for 5 m samples ($p<0.001$).

220

221



222 3.2 Interannual variation in TEP and CSP at station ALOHA

223

224

225

226

227

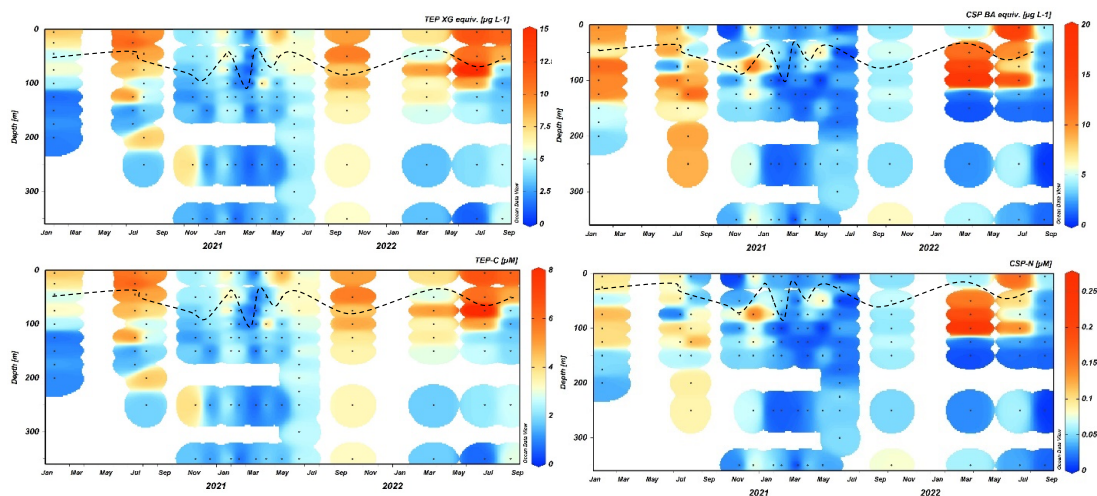
228

229

230

231

232



233

234

235

Figure 2. Time series of TEP and CSP measured in xanthan gum (XG) and bovine albumen (BA) equivalents per litre (top) and converted to $\mu\text{M C}$ and $\mu\text{M N}$ (bottom) at station ALOHA. Dashed line shows mixed layer depth calculated from HOT CTD data as 0.125°C decrease in temperature from the 10 m value.

236

237

238

239

240

241

242

243

244

245

246

At station ALOHA, TEP concentrations were highest during the summer months where values peaked in surface waters ($8 - 15 \text{ XG eq L}^{-1}$; $4 - 8 \mu\text{M C}$), with decreasing TEP concentrations below the SCM to underlying mesopelagic water ($1 - 5 \text{ XG eq L}^{-1}$; $0.5 - 3 \mu\text{M C}$; Figure 2). TEP concentrations were generally lower ($2 - 7 \text{ XG eq L}^{-1}$; $1 - 4 \mu\text{M C}$), with less pronounced vertical gradients during winter months, suggesting either export of accumulated TEP from surface waters or a background of non-seasonal production or abiotic formation in deeper waters. Moderate concentrations of TEP ($3 - 6 \text{ XG eq L}^{-1}$; $2 - 3 \mu\text{M}$) were observed below both the surface mixed layer and above the sub-surface chlorophyll maximum (SCM) (110-130 m) throughout most of the sampling period. Interannual variation in TEP concentrations is approximately $\pm 15 - 40\%$, with May – July 2021 having lower concentrations than similar periods in 2020 and 2022, and March 2021 exhibiting the lowest upper 100 m concentrations (coinciding with deepening of the SML to 110 m after a series of storms and heavy rainfall).

247

248

249

250

251

252

253

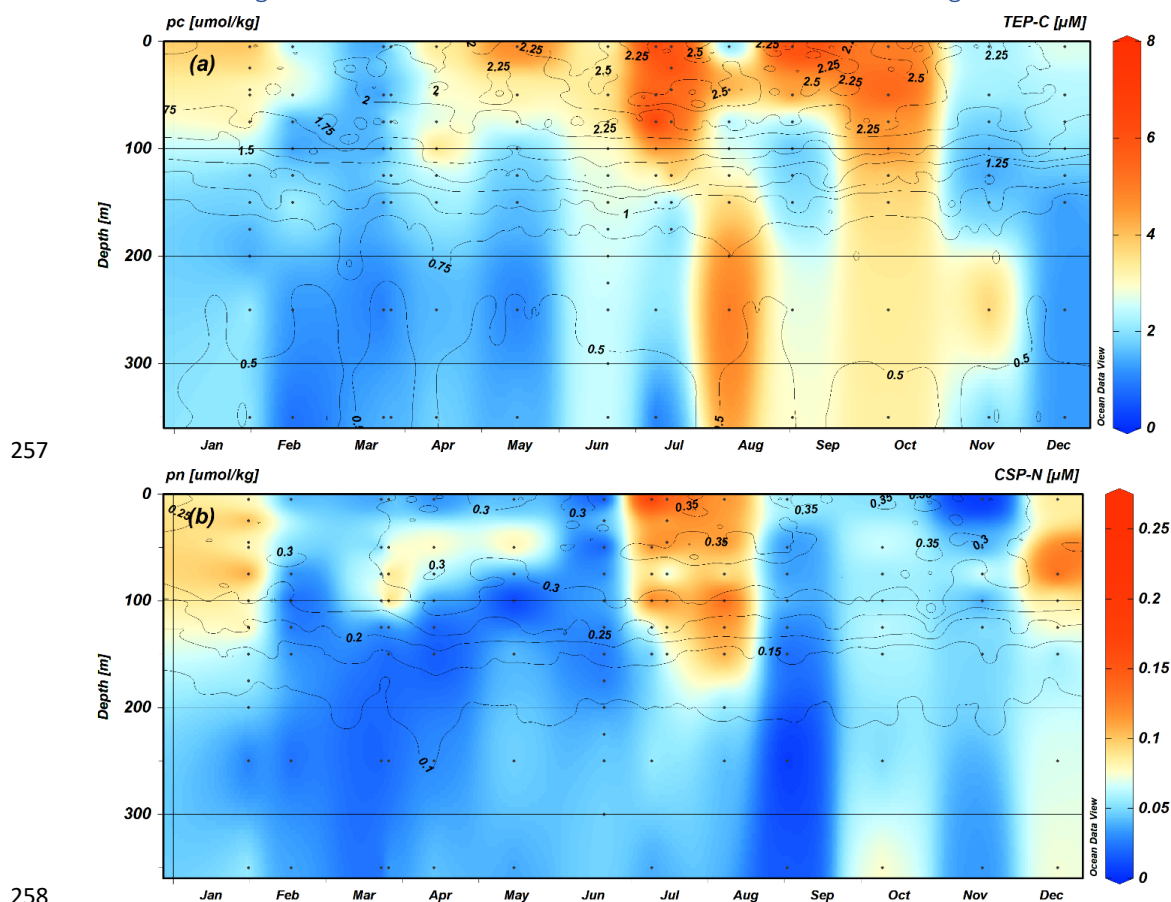
254

CSP distribution at station ALOHA was more variable than TEP, with less distinct vertical gradients and greater interannual variation at specific depths (Figure 2). CSP concentrations appear to be distributed differently to TEP with high concentrations ($6 - 18 \text{ BA eq L}^{-1}$; $0.1 - 0.2 \mu\text{M N}$) below the SML (50 – 100 m) and around the top of the SCM (100-125 m), consistent with the general distributions measured by Cisternas-Novoa et al. (2015) for the Sargasso Sea. CSP in 2021 was $2 - 8 \text{ BA eq L}^{-1}$; $0.01 - 0.07 \mu\text{M N}$ throughout the upper 300 m, similar to sub-SCM and mesopelagic ($>125 \text{ m}$) CSP concentrations in 2020 and 2022, lacking an upper ocean seasonal peak (Fig. 2). As with TEP, CSP concentrations were observed to be greater in March 2022 than post-storms in March 2021.

255



256 3.3 Climatologies of TEP-C and CSP-N with Particulate Carbon and Nitrogen



259 Figure 3. TEP-C (a) and CSP-N (b) (μM) concentration climatologies for 2020-2022 data measured at station ALOHA
 260 overlaid with contours from climatologies of particulate carbon (a) and particulate nitrogen (b) ($\mu\text{mol kg}^{-1}$) from
 261 the Hawaiian Ocean Time-series dataset (1989-2020 data).

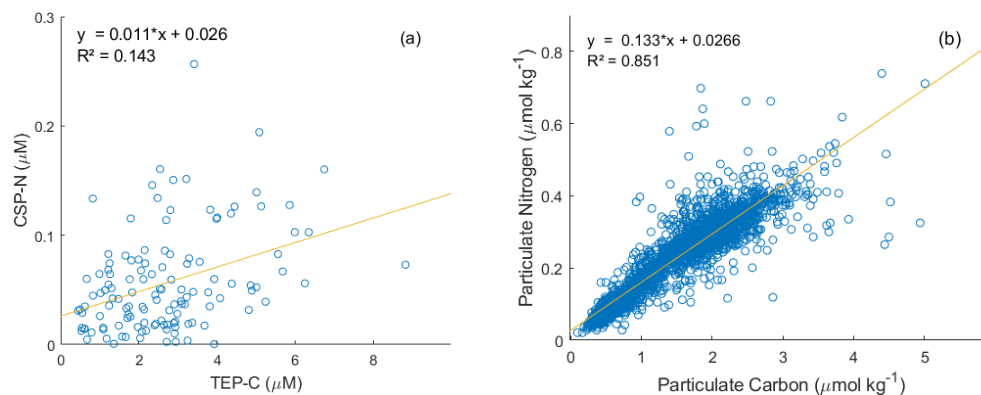
262 TEP exhibits a seasonal pattern with elevated concentrations found in the upper 100 m beginning in
 263 April/May ($3 - 4 \mu\text{M}$) increasing to an annual maximum in late June through early October ($5 - 8 \mu\text{M}$),
 264 followed by a decrease towards an annual minimum in February/March ($1 - 2 \mu\text{M}$) (Fig. 3a). TEP
 265 concentrations below 100 m are $\sim 1 - 2 \mu\text{M}$ from December through June, increasing to $2 - 4 \mu\text{M}$ from
 266 June through November, concurrent with the seasonal maxima in upper 100 m TEP. These moderate
 267 concentrations of TEP below 100 m present during summer/autumn may be due to sinking aggregates as
 268 TEP accumulate through spring-summer and form aggregates before sinking, consistent with the
 269 contemporaneous peak in particulate export rates of $\sim 30\text{-}55 \text{ mg C m}^{-2} \text{ d}^{-1}$ at station ALOHA (Emerson et
 270 al., 1997; Karl et al., 2012; Böttjer et al., 2017; Karl et al., 2021). The CSP climatology suggests two seasonal
 271 concentration maxima in the upper 100 – 130 m occurring in July/August and in December/January (0.07
 272 – $0.13 \mu\text{M}$) (Fig. 3b). CSP concentrations in other months and below these depths are $< 0.06 \mu\text{M}$.
 273 Comparing TEP and CSP concentrations to climatologies of particulate carbon (PC) and nitrogen (PN)



274 respectively at station ALOHA (1989-2020) it is apparent that measured TEP concentrations reflect
 275 variation in euphotic PC more closely than CSP does PN, particularly for samples taken May-October.
 276 Elevated CSP-N concentrations during summer months (0.12-0.24 $\mu\text{M N}$) correspond with PN maxima, but
 277 during winter and spring CSP-N comprises a smaller proportion of PN. While CSP-N values are lower in
 278 magnitude to PN concentrations, TEP-C is frequently observed to exceed background PC concentration at
 279 station ALOHA, which may be an artifact of filtrations for PC and PN analysis losing exopolymers during
 280 GF/F filtration or excess dye binding to particles using the colorimetric method of measuring TEP and CSP
 281 (Passow, 2002b; Bar-Zeev et al., 2011; Annane et al., 2015; Ortega-Retuerta et al., 2019; Nagata et al.,
 282 2021). The difference in nominal pore size between GF/F filters used to sample PC (0.7 μm) and the 0.4
 283 μm pore-size polycarbonate filters used for TEP may also lead to sampling errors when comparing TEP-C
 284 and PC/POC, as most of these particles are small (<3 μm diameter) particularly in the upper 200 m, with
 285 particles tending larger as they age or sink and aggregate through the mesopelagic (Engel et al., 2020). It
 286 is therefore likely that TEP-C to PC ratios are inconsistent with depth and more accurate for samples
 287 containing larger particles. Strands of microgels and larger particles may be easily pulled through GF/F
 288 filters under vacuum pressure and may be disaggregated when sampled in standard sediment catching
 289 methodology due to turbulence, break up at saline density layer, solubilization or rapid remineralization
 290 or preferential consumption by swimmers (Smith et al., 1992; Buesseler et al., 2007; Fawcett et al., 2018).

291 In addition to the variable size spectrum of TEP particles, the electrochemistry that allows the aggregation
 292 of polymers into micro and macroscopic gels (principally divalent cations Ca^{2+} and Mg^{2+}) may be affected
 293 during filtration, and to a different degree with various polycarbonate and GF/F filters (Chin et al., 1998;
 294 Meers et al., 2006). If this is the case, then gels >0.4 μm that would otherwise be retained may be broken
 295 apart into constituent polymers or smaller nanogels that can pass through the filter. This would lead to
 296 TEP being quantified in the DOM fraction and lead to an overestimate of dissolved to particulate fractions
 297 of organic matter.

298 3.4 Patterns of TEP and CSP with respect to particulate C and N at station ALOHA



299

300 Figure 4. Measured CSP-N and TEP-C concentrations within the upper 350 m at station ALOHA from this
 301 study (a) and model II linear regression of particulate nitrogen to particulate carbon from the HOT dataset
 302 (1989-2020 data).

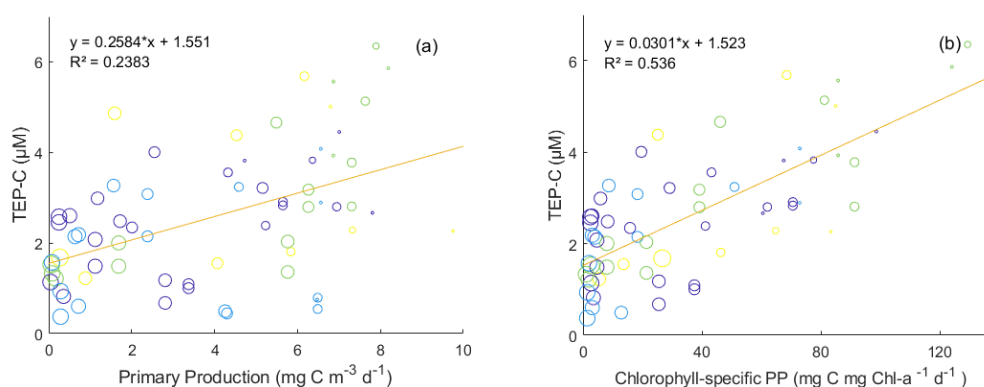
303 Measured PC and PN (Fig. 4) concentrations are well correlated at station ALOHA and the mean C:N ratio
 304 computed from the inverse of the slope (7.55) is slightly higher than the canonical Redfield ratio (6.63),



305 with some deviation at high particulate carbon concentrations and slight relative N-enrichment for most
306 samples from the SCM. In contrast, TEP-C and CSP-N concentrations show very weak correlation or trends
307 at specific sampling depths despite having some periods of similar seasonality and depth distributions
308 through the 2020-2022 sampling period (e.g. elevated upper ocean TEP and CSP during July/August (Fig.
309 2, 3). The weak correlation of TEP-C with CSP-N concentration suggests different formation, consumption,
310 and/or export dynamics for each group of exopolymers.

311

312 3.5 TEP and rates of primary production



313

314 Figure 5. Model II linear regression of TEP-C from this study against same-depth daily primary production (a) and
315 chlorophyll-specific primary production (b) measured at station ALOHA. Circle size indicates depth: larger circles
316 are deeper samples. Colour denotes season: Purple = winter, Blue = Spring, Green = Summer, Yellow = Autumn

317 As TEP production, abiotic formation, and consumption / degradation dynamics are often attributed to
318 phytoplankton community structure and downwelling irradiance intensity (Zamanillo et al., 2019; Bar-
319 Zeev et al., 2011; Ortega-Retuerta et al., 2009a; Berman-Frank et al., 2007; Passow, 2002a), daily primary
320 production (PP) measurements taken during HOT cruises were compared with TEP concentrations,
321 indicating a weak positive correlation for overall PP and a stronger correlation for chlorophyll-normalized
322 PP (Fig. 5). The co-occurrence of higher TEP-C concentrations and high chlorophyll-specific primary
323 production values in surface waters despite nutrient limitation may be indicative of enhanced release of
324 TEP carbohydrate precursors in addition to downregulation of photosynthetic pigment synthesis in light-
325 saturated surface waters (Rabouille et al., 2017; Thompson et al., 2018). The highest values of primary
326 productivity and TEP concentration (>4 µM) were observed in Summer and Fall samples. There are too
327 few data to determine whether TEP-C to PP ratios vary with season. CSP-N showed no such correlation
328 with primary production within this dataset. Although these results may be expected simply from the
329 vertical gradients observed in TEP at station ALOHA and across the June '21 transect, chlorophyll-
330 normalized PP gives some information on whether TEP concentrations are only associated with surface
331 accumulation or formation around peak microbial biomass around the SCM. While this small dataset of
332 TEP and PP matchups may indicate TEP production is occurring around the SCM owing to moderate
333 chlorophyll-normalized PP and TEP concentrations at these depths, there are too few data at present to
334 draw firm conclusions, particularly for near-surface water. Wurl et al. (2011) found a similar disconnect
335 between microbial activity and exopolymer distributions: variations in measured TEP production rates



336 across different Pacific waters (including late-summer samples from station ALOHA) were not associated
337 with phytoplankton blooms, changes in chlorophyll concentrations or fluorescence, with abiotic formation
338 of TEP easily maintaining observed concentrations in the surface mixed layer ($8\text{-}12 \mu\text{M C L}^{-1} \text{d}^{-1}$).

339

340

341 3.6 TEP and CSP concentrations on June '21 transect 22.75°N to 31°N

342

343

344

345

346

347

348

349

350

351

352

353

354

355

356

357

358

359

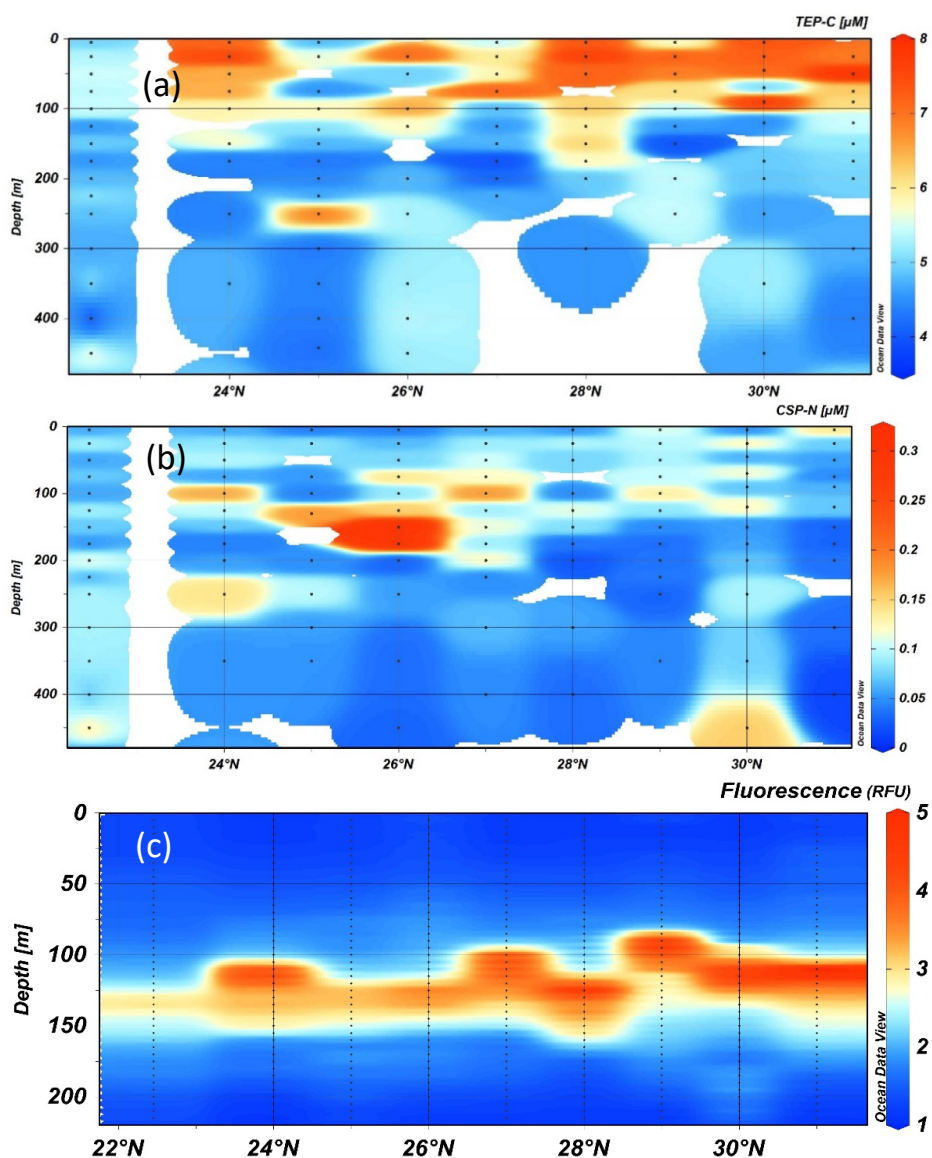
360

361

362

363

364





365 Figure 6. TEP-C (a), CSP-N (b) concentrations and CTD-mounted fluorescence (c) measured during the June 2021
366 transect from 22.75°N to 31°N along ~158°W.

367 Transects of TEP-C and CSP-N in the upper 450 m taken between 22.75°N and 31°N along ~158°W (Fig. 6)
368 during June 2021 show an increase in surface TEP concentrations towards the gyre centre, with two
369 occupations of station ALOHA at the beginning and end of the transect, separated by ten days having the
370 lowest integrated TEP concentrations and degree of vertical gradient. From 24-31°N all stations exhibited
371 pronounced vertical gradients in TEP concentrations between the surface and below the SCM on the order
372 of ~2-3 μM TEP-C. At stations 24°N and 28°N, moderate TEP-C concentrations (5.5 – 7 μM) extended into
373 the SCM whereas high concentrations (6 – 8 μM) were restricted to the upper 75 m at 29°N and 31°N. It
374 is unclear whether this difference is attributable to the production of buoyant TEP in the SCM, varying
375 depths of TEP consumers, surface turbulence from wind forcing, transient variations such as
376 phytoplankton nutrient or oxidative stress, or photoacclimation responses and concomitant exudate
377 production between sites (Sun et al., 2018; Prairie et al., 2019). It is also of note that most stations
378 exhibited a local increase in TEP-C at ~10-20 m immediately above the top of the SCM. The surface
379 maxima in TEP-C present at 28-31°N was ~8 μM (Fig. 6a), similar in magnitude to the surface maxima
380 accumulating seasonally in the station ALOHA time-series (Fig. 2; 3a). However, the vertical TEP-C
381 gradients encountered from 24-31°N in June 2021 were ~2-3 μM , approximately half that observed
382 seasonally at station ALOHA (Fig. 2). The observed ~2 μM latitudinal gradient in 0-100 m TEP-C
383 concentration may also be attributed to the build-up of less labile or less export-prone (or coagulation
384 efficient) TEP as waters move towards the gyre interior (Mari et al., 2007; Rochelle-Newall et al., 2010;
385 Mari et al., 2017), a feature that is also observed for the marine DOC pool (Hansell et al., 2009).

386 Distributions of CSP-N throughout the transect did not correspond to those of TEP-C (Fig. 6). CSP-N
387 concentrations were highest (0.15-0.26 μM) between 75-200 m for stations 24-29°N. Profiles at 22.75°N,
388 30°N and 31°N were more uniform with moderate CSP-N concentrations (0.05 – 0.12 μM) observed below
389 250 m. CSP appears to be more closely associated with peak fluorescence signals (Fig. 6c) while TEP is
390 most abundant in the surface. This disconnect between TEP and CSP distributions suggests different
391 dynamics in formation, residence time and decomposition and export process between the two classes
392 of exopolymers (Grossart et al., 2006; Engel et al., 2015; Thornton, 2018).

393 Previous observations of TEP and CSP particle concentrations in high latitude oceans and temperate shelf
394 seas have observed that both exopolymers are coupled to chlorophyll distributions (Beauvais et al., 2003;
395 Busch et al., 2017; Nosaka et al., 2017; Anastasi, n.d.; von Jackowski et al., 2020). Other mid-latitude
396 regions such as the Sargasso Sea (Cisternas-Novoa et al., 2015) and Catalan Sea (Zamanillo et al., 2021)
397 exhibit different dynamics, where TEP is disconnected from CSP distributions as was observed in this study
398 in the subtropical North Pacific.

399 The seasonal, interannual and latitudinal variation of TEP and CSP observed in this study reinforces the
400 building evidence that exopolymer production, accumulation and remineralization are not static
401 processes, even in oligotrophic regions (Radić et al., 2006; Cisternas-Novoa et al., 2015; Engel et al., 2015;
402 Zäncker et al., 2017). Further process experiments that incorporate TEP and CSP dynamics with respect to
403 other biological and chemical parameters are needed to understand the biogeochemistry of each
404 exopolymer type for a given location and season, aiding efforts to model both with respect to other
405 parameters through depth and time at a synoptic scale.

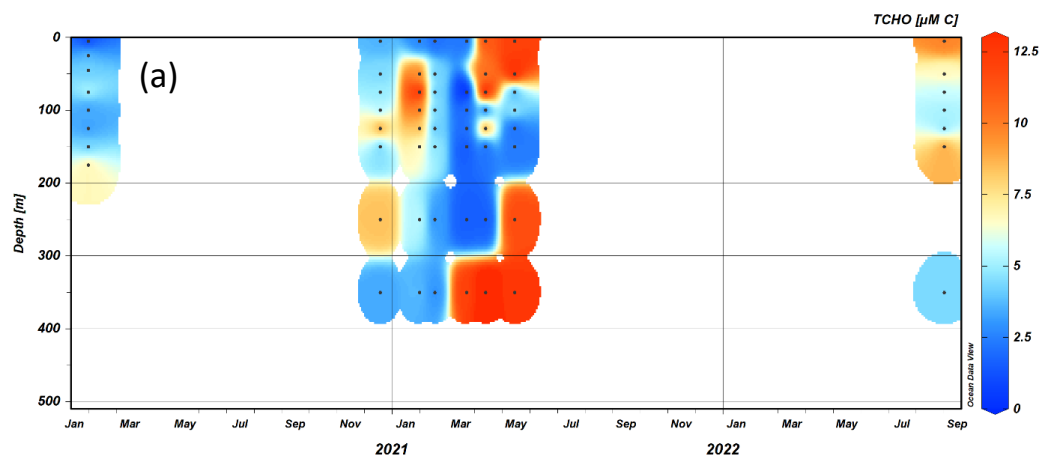


406 In addition to observations and estimates of water-column exopolymer distributions and cycling, the
 407 importance of the sea-surface microlayer to regional TEP and CSP dynamics and seasonal variations is
 408 worthy of consideration in this oligotrophic region, where surfactants are significantly enriched from
 409 underlying surface waters despite low surface PP (Wurl et al., 2011a). Surface microlayer CSP enrichment
 410 factors are often higher than for TEP (Aller et al., 2017; Zäncker et al., 2017), such that any subsequent
 411 bias in the surface mixed layer exopolymer budget may be inconsistent for TEP and CSP. Loss factors
 412 associated with aerosolization and photooxidation of exopolymers from the enriched surface microlayer
 413 are another consideration in quantifying the fate of exopolymers and thus fluxes of organic carbon from
 414 non-photosynthetic DIC uptake (Aller et al., 2017; van Pinxteren et al., 2022).

415 3.7 Dissolved carbohydrates

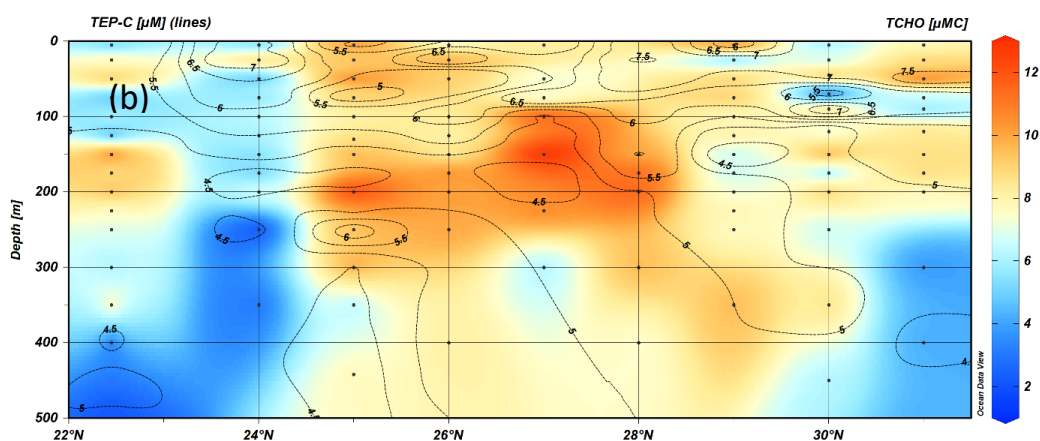
416 Measured concentrations of total dissolved carbohydrates (TCHO) varied between ~2.5-13 μM carbon
 417 equivalents across the June 2021 transect. TCHO distributions did show some overlap with elevated
 418 surface TEP concentrations but were not consistent with TEP concentrations below the surface mixed
 419 layer (Fig. 7b). At many stations, [TCHO] were elevated (9-12.5 μM) around and below the SCM, where
 420 [TEP-C] was low (4.5-5.5 μM).

421



422

423 Figure 7. Reduced time series of total dissolved carbohydrates (TCHO) (μM C) at station ALOHA 2020-2021 (a).





424 Transect of TCHO concentrations during the June 2021 transect from 22.75°N to 31°N overlaid with contours of
425 TEP-C for comparison (b).

426 Most stations exhibited vertical gradients between surface or SCM maxima ($\geq 10 \mu\text{M}$) and reduced [TCHO]
427 ($2 - 8 \mu\text{M}$) below 250 m, but some stations were more consistent with depth (24°N, 29°N) with peak values
428 near the surface. These patterns are generally dissimilar to TEP distributions that are elevated in surface
429 waters.

430 Carbohydrate samples were taken on fewer HOT cruises than TEP and CSP samples during 2020-2022,
431 with the only summer data being from the transect cruise. There is a marked difference in the
432 concentrations and distribution of TCHO between winter samples in 2020 and 2021 where surface
433 concentrations were low ($2 - 6 \mu\text{M}$) and data from spring, where concentrations are consistently high at
434 350 m and in the upper 50 m from April ($> 10 \mu\text{M}$). Compared to DOC measurements taken at station
435 ALOHA, this spring maximum at 350 m seems erroneous, but falls within the intra-annual variability of
436 DOC at 350 m at ALOHA ($\pm 6 \mu\text{M C}$) and monthly variation in particulate export (Karl et al., 2021). It may
437 be possible that some hydrolysable particulate polysaccharides are drawn through combusted GF/F filters
438 (Nagata et al., 2021). Another potential explanation is the degradation and/or solubilization of
439 exopolymers below the SCM where polysaccharide-specific enzyme activity is elevated (Reintjes et al.,
440 2020).

441 Measurements from this study were on the lower end of marine dissolved carbohydrate measurements,
442 but consistent with previous measurements taken within the subtropical North Pacific (Pakulski and
443 Benner, 1994), 30-60% lower than observed across the subtropical Atlantic (Burney et al., 1979; Goldberg
444 et al., 2010) and 40-100% higher than in the Bay of Bengal and Arabian Sea (Bhosle et al., 1998).

445 The observed disconnect between TEP and TCHO distributions may be attributed to both formation and
446 degradation processes: precursors being created around the SCM by phytoplankton and resultant low-
447 density TEP particles concentrating in surface waters or sinking TEP being hydrolyzed below the SCM by
448 bacteria, yielding reduced TCHO concentrations. The latter process is consistent with the hypothesized
449 remineralization of low-N organic matter requiring heterotrophic nitrate uptake, generating a negative
450 preNO_3^- anomaly (Fawcett et al., 2018), but would require compositional analysis of TEP particles,
451 dissolved sugars, and stable isotopic measurements of the relevant nutrient and organic matter N
452 contents through the upper 400 m to confirm. Lastly, a lack of spatiotemporal coherence in the
453 distributions of TEP and its precursor TCHO may result from differing timescales over which they are
454 biotically cycled, with the latter possibly processed 3-10 times faster than other common labile organic
455 materials like amino acids by bacteria in open ocean environments (Kaiser and Benner, 2012), enabled by
456 a complex suite of bacterial enzymes for hydrolyzing polysaccharides and transporting carbohydrates into
457 cells' periplasm (Reintjes et al., 2020).

458 3.8 Contribution of TEP production to net community production and PreNO_3^- anomalies

459 Here we use the seasonal study of TEP distributions from the upper 350 m at station ALOHA to quantify
460 its potential contribution to help explain the dual enigmas of significant net community production from
461 the mixed layer in the absence of large vertical nutrient inputs and the generation of PreNO_3^- anomalies
462 within and immediately below the euphotic zone of the subtropical North Pacific. The potential
463 contribution of TEP to surface excess DIC drawdown and sub-SCM negative preformed nitrate anomalies
464 under nutrient limitation has been identified through field and lab observations, and modelling efforts
465 (Mari et al., 2017; Fawcett et al., 2018; Letscher and Villareal, 2018; Nagata et al., 2021). The $\sim 4-6 \mu\text{M}$



466 TEP-C concentration gradient observed between Apr-Oct in the upper 100 m in this study, representative
467 of the euphotic zone above the SCM at station ALOHA, and the ~100 – 300 m layer representative of the
468 SCM and the upper mesopelagic, may account for a significant contribution of TEP to both the seasonal
469 mixed layer dissolved inorganic carbon drawdown (NCP) and upper ocean preNO_3^- anomalies through the
470 processes of TEP production, sinking or matter exported during winter mixing, and subsequent
471 remineralization at depth. TEP may have a significant role in exporting low-N organic matter to underlying
472 waters, particularly during the summer to early autumn months (Fig. 3) when the seasonal maximum in
473 upper 100 m TEP concentrations extends vertically into the 100 – 300 m layer, suggestive of vertical
474 sinking.

475 The 4-6 μM vertical TEP gradient that arises seasonally reported here, e.g. 5-8 μM in the upper 100 m
476 Apr-Oct decreasing to 1-2 μM below, is higher than those observed by Cisternas-Novoa et al (2015)
477 (~10 $\mu\text{g XG eq. L}^{-1}$ / ~0.5 $\mu\text{M TEP-C}$) in the Sargasso Sea and Wurl et al. (2011) (1.4-3.2 $\mu\text{M TEP-C}$ with
478 one high-TEP station with a gradient of 27 $\mu\text{M TEP-C}$) in the subtropical North Pacific when applying the
479 carbon-converted units measured in this study. The wintertime erasure in vertical TEP gradients between
480 the surface and 200 m is observed in Feb-Mar and Nov-Dec samples from station ALOHA in this study (Fig.
481 3a), supporting the hypothesis of TEP-C export to depth of ~100 m at ALOHA and possibly deeper at
482 latitudes further north in the subtropical North Pacific that may facilitate seasonal TEP export (beyond
483 sinking aggregates which may occur year-round). As carbon conversion factors for TEP at station ALOHA
484 are consistent for summer and autumn, it seems that exported TEP from the SML to depths below may
485 be assumed to have consistent carbon content, whether it is sinking at any time of the year or exported
486 during winter mixing, contributing to positive and negative preNO_3^- anomalies at consistent C:O₂
487 stoichiometry. However, the C:N ratio of TEP and CSP does appear to vary from highly carbon rich in
488 summer, to less carbon rich in autumn, meaning respiration associated with sinking exopolymers may
489 have variable O₂ drawdown to nitrate release throughout the year.

490 The background particulate carbon flux at 150 m measured at station ALOHA of $27.8 \pm 9.7 \text{ mg C m}^{-2} \text{ d}^{-1}$
491 ($845 \pm 295 \text{ mmol C m}^{-2} \text{ yr}^{-1}$; Karl et al. 2021) would seem to indicate that the export of even a portion of
492 the 0-150 m integrated $750 \pm 150 \text{ mmol C m}^{-2}$ summer/fall TEP stock by either TEP sinking or vertical
493 export following winter mixing would be a significant flux of carbon on an annual scale. Furthermore,
494 sediment trap data indicate that particulate matter exported at station ALOHA is typically slightly above
495 Redfieldian C:N proportions, e.g. ~8.0 (Hannides et al., 2009), while TEP measured in this study varied
496 between 16.4 in October to 34.3 in June (Table 1). The annual NCP rate estimated from the seasonal DIC
497 cycle within the mixed layer (~50 m) at Station ALOHA is $2.3 \pm 0.8 \text{ mol m}^{-2} \text{ yr}^{-1}$ (Keeling et al., 2004), thus
498 the annual production of a surface accumulated excess TEP-C stock of 0.2-0.3 mol m^{-2} in the upper 50 m
499 ($\Delta\text{TEP} = 4 - 6 \mu\text{M} \times 50 \text{ m}$) may contribute 6.5-20% of the overall NCP estimated from DIC drawdown ($1.5-$
500 $3.1 \text{ mol m}^{-2} \text{ yr}^{-1}$).

501 From the calculation above, TEP production within and subsequent export below the surface mixed layer
502 may explain up to 20% of the total NCP, but how does this estimate compare to the estimates of 'excess'
503 DIC drawdown, that is DIC drawdown in excess of known N inputs, at this site? For this calculation, it is
504 helpful to compute the N demand required to produce the observed NCP rate, partitioned amongst the
505 relative proportions of POM, DOM, and TEP production. Johnson et al. (2010) computed a total N demand
506 of $287 \text{ mmol N m}^{-2} \text{ yr}^{-1}$ at station ALOHA assuming total organic matter production followed a C:N
507 stoichiometry of 8.0, matching the sinking POM stoichiometry. Letscher & Villareal (2018) empirically
508 determined the fraction of NCP partitioned to DOM at station ALOHA from tracer budgets in upper



509 mesopelagic isopycnal layers from the station ALOHA climatology, finding that ~50% of NCP is exported
 510 as DOM. We have computed the mean DOM C:N stoichiometry in the upper 200 m at 15.5 ± 1.3 from the
 511 same climatology. Assuming NCP is partitioned 50/50% between POM and DOM with C:N stoichiometries
 512 of 8.0 and 15.5 respectively, we compute a revised N demand of $218 \text{ mmol N m}^{-2} \text{ yr}^{-1}$ to satisfy the observed
 513 $2.3 \text{ mol C m}^{-2} \text{ yr}^{-1}$ NCP within the mixed layer. Johnson et al. (2010) summarized total N supply to the mixed
 514 layer at station ALOHA finding a magnitude of $144 - 201 \text{ mmol N m}^{-2} \text{ yr}^{-1}$. Thus approximately 8 – 34%
 515 (mean = 21%) of the observed NCP N requirement is not accounted for by the known N supply for the
 516 scenario where only POM and DOM production contribute to NCP. Our estimate of TEP production and
 517 its contribution to NCP at this site is 6.5 – 20%, with an observationally determined C:N stoichiometry of
 518 $16.4 - 34.3$ (Table 1). Addition of TEP into the mixed layer NCP budget yields an N demand to explain TEP
 519 production of $4 - 28 \text{ mmol N m}^{-2} \text{ yr}^{-1}$, which reduces the total N demand to $174 - 208 \text{ mmol N m}^{-2} \text{ yr}^{-1}$.
 520 Comparing this N demand to the prior calculated N demand that included POM and DOM but ignored TEP,
 521 TEP contributions to the upper ocean NCP budget help explain ~57% of the unexplained ‘excess DIC
 522 drawdown’ from the mixed layer, reducing the overall unexplained drawdown from a mean of ~21% to
 523 ~9%.

524 Table 2. Estimates of the nitrogen demand partitioned amongst POM, DOM, and TEP required to satisfy each
 525 fractional contribution (f_{NCP}) of the mixed layer $2.3 \text{ mol m}^{-2} \text{ yr}^{-1}$ NCP at station ALOHA using their respective C:N
 526 stoichiometries. Total N supply is taken from Johnson et al. (2010) and includes vertical NO_3 fluxes plus N_2 fixation.
 527 $f_{\text{NCP}_{\text{POM}}}$ varies as the particulate fraction not attributable to TEP or DOM ($f_{\text{NCP}_{\text{POM}}} = 1 - (f_{\text{NCP}_{\text{TEP}}} + f_{\text{NCP}_{\text{DOM}}})$), POM C:N
 528 from Hannides et al. (2009), $f_{\text{NCP}_{\text{DOM}}}$ from Letscher and Villareal (2018), DOM C:N from the upper 200 m average of
 529 the station ALOHA climatology, $f_{\text{NCP}_{\text{TEP}}}$ and TEP C:N (Table 1) from this study.

Depth integration		f_{NCP}	C:N	N demand ($\text{mmol N m}^{-2} \text{ yr}^{-1}$)	% of N demand
50m	POM	0.30-0.435	8	86-125	36-52
	DOM	0.5	15.5	74	31
	TEP	0.065-0.20	16.4-34.3	4-28	2-12
	Total demand			174-208	
	Total supply			144-201	

530

531 Lastly, we compare the seasonal TEP cycle observed at station ALOHA from 2020-2022 to previous
 532 estimates of the formation rates of residual PreNO_3^- anomalies within and immediately below the
 533 euphotic zone. Letscher and Villareal (2018) estimated the seasonal (~Apr-Oct) development of a residual
 534 positive PreNO_3^- (rPPN) anomaly (i.e. the residual anomaly after accounting for non-Redfield POM and
 535 DOM stoichiometry) within the upper 100 m with a climatological magnitude of $0.53 \pm 0.27 \mu\text{M}$. A similar
 536 seasonal negative PreNO_3^- (rNPN) anomaly develops between ~100-150 m with a climatological
 537 magnitude of $-0.54 \pm 0.25 \mu\text{M}$ over a ~180-day period from Apr-Oct, consistent with surface TEP
 538 accumulation before winter mixing (Fig. 2). With assumed 1:1 C to O_2 stoichiometry of TEP formation and
 539 remineralization (as for nearly pure carbohydrate material), the consumption of 4-6 μM TEP C (at a C:N
 540 ratio of 25 ± 8) should release the equivalent of 0.12-0.35 μM NO_3^- which is 23-67% of the 0.53 μM rNPN
 541 and 22-64% of the 0.54 μM rPPN mean anomalies. These values for TEP’s potential contribution to rNPN
 542 assume the export of surface TEP to underlying waters 100-200 m where they are efficiently
 543 remineralized. If a large proportion of seasonal TEP production is quickly exported to the deeper



544 mesopelagic through aggregation and gravitational settling or winter mixing, then these values will likely
545 be overestimates. Remaining mechanisms to explain the remainder of rPPN/rNPN anomaly formation
546 include mining of sub-euphotic zone nitrate by vertically migrating phytoplankton (Pilskaln et al., 2005;
547 Villareal et al., 2014) and heterotrophic bacterial uptake of nitrate when consuming C-rich organic matter
548 such as TEP (Fawcett et al., 2018).

549 Finally, we note that moderate concentrations of TEP at 250 and 350 m (2-3 $\mu\text{M C}$) are present throughout
550 the year at station ALOHA, but whether these concentrations represent matter exported from the surface
551 or SCM below the depth of the rNPN anomaly ($\sim 100 - 175$ m; Letscher & Villareal, 2018), or separate
552 activity in the upper mesopelagic is unclear. Compositional analysis of TEP molecules and polysaccharide-
553 associated enzymes throughout the water column and over an annual cycle may elucidate sources and
554 sinks of TEP beyond physical sinking and mixing processes.

555 4 Conclusions

556 Exopolymers measured in the subtropical North Pacific were found to have seasonal and latitudinal
557 variability, with elevated concentrations in surface waters for TEP and around the SCM for CSP. The
558 seasonality and vertical distributions of TEP and CSP were not correlated, suggesting different production
559 and loss processes in this region. While TEP concentrations were low compared to other regions, their
560 highly carbon-enriched stoichiometry (particularly in summer with C:N = 26-38) means that these particles
561 are a significant component of the euphotic POC pool. A summertime transect from 22.75° to 31°N in the
562 North Central Pacific indicated that TEP concentrations increased towards the gyre interior, though
563 without additional data on TEP molecular composition it is difficult to ascertain whether this is
564 accumulation of more refractory TEP, or enhanced production/depressed export in these waters. The
565 seasonal and latitudinal variation we observed in carbon and nitrogen conversion factors suggest using a
566 single factor will bias many estimates of TEP-C and CSP-N from dye-binding assays. We therefore hope
567 that more effort will be made in future studies to constrain TEP and CSP elemental stoichiometry to
568 compare exopolymer concentrations from different depths, seasons and locations with greater
569 confidence. TEP concentrations measured with the Alcian blue spectrophotometric method and
570 converted to $\mu\text{M C}$ with our empirically derived CCF were found to be greater than GF/F collected
571 particulate carbon measurements. Additionally, the estimated C:N stoichiometry of 16.4 – 38.1 for TEP
572 from this study is significantly C-rich/N-poor relative to the C:N of the sinking flux collected in sediment
573 traps at station ALOHA, 8.0 (Hannides et al., 2009). This supports the hypotheses that TEP and marine
574 microgels may be ‘missed’ by traditional sampling techniques for sinking and suspended particulate
575 organic carbon, possibly due to disaggregation of the gel-particles upon encountering the GF/F filter or
576 collection brine of sediment traps as well as potential rapid microbial remineralization within trap cups
577 (Fawcett et al., 2018 and references therein). Future research is required to resolve the mechanisms
578 leading to inefficient collection of TEP within standard marine particle sampling protocols and fully
579 integrate TEP and marine gels sampling within marine carbon biogeochemistry studies.

580 Measurements of dissolved carbohydrates, the precursors to TEP formation, exhibited less consistent
581 spatiotemporal trends and were generally not correlated with TEP with concentrations being elevated
582 around and below the SCM during the summertime transect for some stations, but concentrated in
583 surface waters at others. There are too few data available from our time series to assess annual variations
584 confidently. Although only measured in low concentrations (2.5-13 μM) vs total DOC pools at station
585 ALOHA (55-75 μM), the presence of this labile substrate below the SCM means compositional analysis of



586 these carbohydrates and exported TEP may elucidate the importance of TEP remineralization to this pool
587 of DOM and the oxygen demand TEP and TCHO cycling requires.

588 The dataset presented here marks a contribution to quantifying the role of exopolymers to euphotic and
589 upper mesopelagic biogeochemistry in the subtropical North Pacific that can be expanded on with
590 complimentary measurements and analyses of composition, carbon budgets and formation, export and
591 cycling rates. Work that helps to validate the sources and sinks of exopolymers within the water column
592 is particularly important in quantifying how much carbon is exported from or cycled within surface waters
593 (including the surface microlayer) and where these molecules are remineralized. Compositional analysis
594 of TEP particle and dissolved carbohydrates compositions and associated proteomic or transcriptomic
595 analyses may elucidate the vertical distribution of TEP production, enzymatic hydrolyzation and
596 remineralization of the resulting labile monomeric sugars.

597 Following the conversion of semi-quantitative measurements of exopolymers from dye-binding assays,
598 our elemental conversions to C and N units allow us to estimate the magnitude of TEP's importance to
599 surface ocean carbon dynamics on an annual cycle. We estimate that TEP accumulation within the ~50 m
600 mixed layer may constitute 6.5-20% ($0.2-0.3 \text{ mol m}^{-2} \text{ y}^{-1}$) of the NCP ($2.3 \pm 0.8 \text{ mol m}^{-2} \text{ y}^{-1}$) at station ALOHA.
601 With its low N requirement, TEP reduces the overall N demand needed to explain the observed NCP at
602 this site, bringing the measured N supply and demand into near balance. If TEP is sufficiently exported
603 below the euphotic zone by a combination of sinking and/or winter vertical mixing, its cycling can reduce
604 the unexplained 'excess' DIC drawdown from the mixed layer by ~60%, bringing the overall unexplained
605 excess (or missing N supply) to ~9%.

606 Though TEP sinking rates, remineralization rates and $\text{C}:\text{O}_2$ respiration stoichiometry are not addressed in
607 this dataset, previous studies in analogous regions indicate that the summertime production of highly
608 non-Redfieldian exopolymers and potential winter export observed in this time series may explain a
609 significant portion of subtropical positive and negative PreNO_3^- anomalies (22-67%), consistent with this
610 mechanism's description and modelling by Letscher and Villareal (2018). Uncertainty in the contribution
611 of TEP to PreNO_3^- anomalies (and excess DIC drawdown) primarily results from variability in the total TEP
612 upper ocean accumulation and its C:N ratio; with some evidence for seasonal, vertical, and latitudinal
613 differences in these ratios evidenced in this study (Table 1). More frequent measurements of TEP
614 concentrations and its stoichiometry from the subtropical North Pacific and elsewhere would help
615 quantify the magnitude and causes of this variability.

616

617

618

619 **Author contributions**

620 RTL and TV conceptualized this study as part of NSF grants 1923687 and 1923667 "Transparent
621 exopolymer and phytoplankton vertical migration as sources for preformed nitrate anomalies in the
622 subtropical N. Pacific Ocean". KC, RTL, and HOT technicians performed fieldwork; KC performed
623 laboratory analyses for TEP, CSP and TCHO and respective data analyses. KC, RTL, and TV contributed to
624 writing and editing. Data from the Hawaiian Ocean Time series were obtained via the Hawaii Ocean Time-



625 series HOT-DOGS application; University of Hawai'i at Mānoa. National Science Foundation Award #
626 1756517.

627 **Acknowledgements**

628 We would like to thank the crew and technicians aboard RV Kilo Moana for their assistance in collecting
629 samples through the COVID pandemic and assisting during the June '21 transect cruise. We are grateful
630 to Angelicque White (UH-Manoa) for her assistance and leadership in accommodating the TEP, CSP, and
631 TCHO sampling on the 2020-2022 HOT cruises and to Brandon Brenes (UH-Manoa) for much of the sample
632 collection at sea. We also wish to thank former UNH graduate students Jessica Gray and Sarah Benson for
633 their assistance with sampling during the 2021 cruise.

634

635 **Financial support**

636 This study was funded as part of NSF grant 1923687 to RTL and 1923667 to TV entitled: "Collaborative
637 research: Transparent exopolymer and phytoplankton vertical migration as sources for preformed nitrate
638 anomalies in the subtropical N. Pacific Ocean."

639

640 **Data availability**

641 The data reported in this study are available at: <https://www.bco-dmo.org/project/772658>.

642

643 **Competing interests**

644 We declare no competing interests in the undertaking and publication of this study.

645

646 **References**

647 Abell, J., Emerson, S., and Keil, R. G.: Using preformed nitrate to infer decadal changes in DOM
648 remineralization in the subtropical North Pacific, *Glob. Biogeochem. Cycles*, 19,
649 <https://doi.org/10.1029/2004GB002285>, 2005.

650 Aller, J. Y., Radway, J. C., Kiltath, W. P., Bothe, D. W., Wilson, T. W., Vaillancourt, R. D., Quinn, P. K.,
651 Coffman, D. J., Murray, B. J., and Knopf, D. A.: Size-resolved characterization of the polysaccharidic and
652 proteinaceous components of sea spray aerosol, *Atmos. Environ.*, 154, 331–347,
653 <https://doi.org/10.1016/j.atmosenv.2017.01.053>, 2017.

654 Anastasi, G.: OBSERVATIONS AND MODELLING OF TRANSPARENT EXOPOLYMER PARTICLES (TEP) AND
655 THEIR ROLE IN CARBON CYCLING IN SHELF SEAS, 237, n.d.

656 Annane, S., St-Amand, L., Starr, M., Pelletier, E., and Ferreyra, G. A.: Contribution of transparent
657 exopolymeric particles (TEP) to estuarine particulate organic carbon pool, *Mar. Ecol. Prog. Ser.*, 529, 17–
658 34, <https://doi.org/10.3354/meps11294>, 2015.



- 659 Arnosti, C., Wietz, M., Brinkhoff, T., Hehemann, J.-H., Probandt, D., Zeugner, L., and Amann, R.: The
660 Biogeochemistry of Marine Polysaccharides: Sources, Inventories, and Bacterial Drivers of the
661 Carbohydrate Cycle, *Annu. Rev. Mar. Sci.*, 13, 81–108, <https://doi.org/10.1146/annurev-marine-032020-012810>, 2021.
- 663 Ascani, F., Richards, K. J., Firing, E., Grant, S., Johnson, K. S., Jia, Y., Lukas, R., and Karl, D. M.: Physical and
664 biological controls of nitrate concentrations in the upper subtropical North Pacific Ocean, *Deep Sea Res. Part II Top. Stud. Oceanogr.*, 93, 119–134, <https://doi.org/10.1016/j.dsr2.2013.01.034>, 2013.
- 666 Azetsu-Scott, K. and Passow, U.: Ascending marine particles: Significance of transparent exopolymer
667 particles (TEP) in the upper ocean, *Limnol. Oceanogr.*, 49, 741–748,
668 <https://doi.org/10.4319/lo.2004.49.3.0741>, 2004.
- 669 Bar-Zeev, E., Berman, T., Rahav, E., Dishon, G., Herut, B., Kress, N., and Berman-Frank, I.: Transparent
670 exopolymer particle (TEP) dynamics in the eastern Mediterranean Sea, *Mar. Ecol. Prog. Ser.*, 431, 107–
671 118, <https://doi.org/10.3354/meps09110>, 2011.
- 672 Beauvais, S., Pedrotti, M. L., Villa, E., and Lemée, R.: Transparent exopolymer particle (TEP) dynamics in
673 relation to trophic and hydrological conditions in the NW Mediterranean Sea, *Mar. Ecol. Prog. Ser.*, 262,
674 97–109, <https://doi.org/10.3354/meps262097>, 2003.
- 675 Berman-Frank, I., Rosenberg, G., Levitan, O., Haramaty, L., and Mari, X.: Coupling between autocatalytic
676 cell death and transparent exopolymeric particle production in the marine cyanobacterium
677 *Trichodesmium*, *Environ. Microbiol.*, 9, 1415–1422, <https://doi.org/10.1111/j.1462-2920.2007.01257.x>,
678 2007.
- 679 Bhosle, N. B., Bhaskar, P. V., and Ramachandran, S.: Abundance of dissolved polysaccharides in the
680 oxygen minimum layer of the Northern Indian Ocean, *Mar. Chem.*, 63, 171–182,
681 [https://doi.org/10.1016/S0304-4203\(98\)00061-9](https://doi.org/10.1016/S0304-4203(98)00061-9), 1998.
- 682 Böttjer, D., Dore, J. E., Karl, D. M., Letelier, R. M., Mahaffey, C., Wilson, S. T., Zehr, J., and Church, M. J.:
683 Temporal variability of nitrogen fixation and particulate nitrogen export at Station ALOHA, *Limnol. Oceanogr.*, 62, 200–216, <https://doi.org/10.1002/lno.10386>, 2017.
- 685 Buesseler, K. O., Antia, A. N., Chen, M., Fowler, S. W., Gardner, W. D., Gustafsson, O., Harada, K.,
686 Michaels, A. F., Rutgers van der Loeff, M., Sarin, M., Steinberg, D. K., and Trull, T.: An assessment of the
687 use of sediment traps for estimating upper ocean particle fluxes, *J. Mar. Res.*, 65, 345–416,
688 <https://doi.org/10.1357/002224007781567621>, 2007.
- 689 Burney, C. M., Johnson, K. M., Lavoie, D. M., and Sieburth, J. McN.: Dissolved carbohydrate and
690 microbial ATP in the North Atlantic: concentrations and interactions, *Deep Sea Res. Part Oceanogr. Res. Pap.*, 26, 1267–1290, [https://doi.org/10.1016/0198-0149\(79\)90068-2](https://doi.org/10.1016/0198-0149(79)90068-2), 1979.
- 692 Busch, K., Endres, S., Iversen, M. H., Michels, J., Nöthig, E.-M., and Engel, A.: Bacterial Colonization and
693 Vertical Distribution of Marine Gel Particles (TEP and CSP) in the Arctic Fram Strait, *Front. Mar. Sci.*, 4,
694 2017.
- 695 Chin, W.-C., Orellana, M. V., and Verdugo, P.: Spontaneous assembly of marine dissolved organic matter
696 into polymer gels, *Nature*, 391, 568–572, <https://doi.org/10.1038/35345>, 1998.



- 697 Chow, C. H., Cheah, W., and Tai, J.-H.: A rare and extensive summer bloom enhanced by ocean eddies in
698 the oligotrophic western North Pacific Subtropical Gyre, *Sci. Rep.*, 7, 6199,
699 <https://doi.org/10.1038/s41598-017-06584-3>, 2017.
- 700 Cisternas-Novoa, C., Lee, C., and Engel, A.: Transparent exopolymer particles (TEP) and Coomassie
701 stainable particles (CSP): Differences between their origin and vertical distributions in the ocean, *Mar.*
702 *Chem.*, 175, 56–71, <https://doi.org/10.1016/j.marchem.2015.03.009>, 2015.
- 703 Dave, A. C. and Lozier, M. S.: Local stratification control of marine productivity in the subtropical North
704 Pacific, *J. Geophys. Res. Oceans*, 115, <https://doi.org/10.1029/2010JC006507>, 2010.
- 705 Emerson, S.: Annual net community production and the biological carbon flux in the ocean, *Glob.*
706 *Biogeochem. Cycles*, 28, 14–28, <https://doi.org/10.1002/2013GB004680>, 2014.
- 707 Emerson, S. and Hayward, T.: Chemical tracers of biological processes in shallow waters of North Pacific:
708 preformed nitrate distributions., *J. Mar. Res.*, 53, 499–513, 1995.
- 709 Emerson, S., Quay, P., Karl, D., Winn, C., Tupas, L., and Landry, M.: Experimental determination of the
710 organic carbon flux from open-ocean surface waters, *Nature*, 389, 951–954,
711 <https://doi.org/10.1038/40111>, 1997.
- 712 Engel, A. and Passow, U.: Carbon and nitrogen content of transparent exopolymer particles (TEP) in
713 relation to their Alcian Blue adsorption, *Mar. Ecol. Prog. Ser.*, 219, 1–10,
714 <https://doi.org/10.3354/meps219001>, 2001.
- 715 Engel, A., Borchard, C., Loginova, A., Meyer, J., Hauss, H., and Kiko, R.: Effects of varied nitrate and
716 phosphate supply on polysaccharidic and proteinaceous gel particle production during tropical
717 phytoplankton bloom experiments, *Biogeosciences*, 12, 5647–5665, <https://doi.org/10.5194/bg-12-5647-2015>, 2015.
- 719 Engel, A., Endres, S., Galgani, L., and Schartau, M.: Marvelous Marine Microgels: On the Distribution and
720 Impact of Gel-Like Particles in the Oceanic Water-Column, *Front. Mar. Sci.*, 7,
721 <https://doi.org/10.3389/fmars.2020.00405>, 2020.
- 722 Fawcett, S. E., Johnson, K. S., Riser, S. C., Van Oostende, N., and Sigman, D. M.: Low-nutrient organic
723 matter in the Sargasso Sea thermocline: A hypothesis for its role, identity, and carbon cycle implications,
724 *Mar. Chem.*, 207, 108–123, <https://doi.org/10.1016/j.marchem.2018.10.008>, 2018.
- 725 Goldberg, S. J., Carlson, C. A., Bock, B., Nelson, N. B., and Siegel, D. A.: Meridional variability in dissolved
726 organic matter stocks and diagenetic state within the euphotic and mesopelagic zone of the North
727 Atlantic subtropical gyre, *Mar. Chem.*, 119, 9–21, <https://doi.org/10.1016/j.marchem.2009.12.002>,
728 2010.
- 729 Grossart, H.-P., Czub, G., and Simon, M.: Algae–bacteria interactions and their effects on aggregation
730 and organic matter flux in the sea, *Environ. Microbiol.*, 8, 1074–1084, <https://doi.org/10.1111/j.1462-2920.2006.00999.x>, 2006.



- 732 Gruber, N., Keeling, C. D., and Stocker, T. F.: Carbon-13 constraints on the seasonal inorganic carbon
733 budget at the BATS site in the northwestern Sargasso Sea, *Deep Sea Res. Part Oceanogr. Res. Pap.*, 45,
734 673–717, [https://doi.org/10.1016/S0967-0637\(97\)00098-8](https://doi.org/10.1016/S0967-0637(97)00098-8), 1998.
- 735 Guo, S., Wu, Y., Zhu, M., and Sun, X.: Concentrations of transparent exopolymer particles (TEPs) and
736 their role in the carbon export in the South China Sea and western tropical North Pacific, *Mar. Environ.*
737 *Res.*, 179, 105699, <https://doi.org/10.1016/j.marenvres.2022.105699>, 2022.
- 738 Hannides, C. C. S., Popp, B. N., Landry, M. R., and Graham, B. S.: Quantification of zooplankton trophic
739 position in the North Pacific Subtropical Gyre using stable nitrogen isotopes, *Limnol. Oceanogr.*, 54, 50–
740 61, <https://doi.org/10.4319/lo.2009.54.1.0050>, 2009.
- 741 Iuculano, F., Mazuecos, I. P., Reche, I., and Agustí, S.: Prochlorococcus as a Possible Source for
742 Transparent Exopolymer Particles (TEP), *Front. Microbiol.*, 8, 2017.
- 743 von Jackowski, A., Grosse, J., Nöthig, E.-M., and Engel, A.: Dynamics of organic matter and bacterial
744 activity in the Fram Strait during summer and autumn, *Philos. Trans. R. Soc. Math. Phys. Eng. Sci.*, 378,
745 20190366, <https://doi.org/10.1098/rsta.2019.0366>, 2020.
- 746 Johnson, K. S., Riser, S. C., and Karl, D. M.: Nitrate supply from deep to near-surface waters of the North
747 Pacific subtropical gyre, *Nature*, 465, 1062–1065, <https://doi.org/10.1038/nature09170>, 2010.
- 748 Kaiser, K. and Benner, R.: Organic matter transformations in the upper mesopelagic zone of the North
749 Pacific: Chemical composition and linkages to microbial community structure, *J. Geophys. Res. Oceans*,
750 117, <https://doi.org/10.1029/2011JC007141>, 2012.
- 751 Karl, D. M., Church, M. J., Dore, J. E., Letelier, R. M., and Mahaffey, C.: Predictable and efficient carbon
752 sequestration in the North Pacific Ocean supported by symbiotic nitrogen fixation, *Proc. Natl. Acad. Sci.*,
753 109, 1842–1849, <https://doi.org/10.1073/pnas.1120312109>, 2012.
- 754 Karl, D. M., Letelier, R. M., Bidigare, R. R., Björkman, K. M., Church, M. J., Dore, J. E., and White, A. E.:
755 Seasonal-to-decadal scale variability in primary production and particulate matter export at Station
756 ALOHA, *Prog. Oceanogr.*, 195, 102563, <https://doi.org/10.1016/j.pocean.2021.102563>, 2021.
- 757 Keeling, C. D., Brix, H., and Gruber, N.: Seasonal and long-term dynamics of the upper ocean carbon
758 cycle at Station ALOHA near Hawaii, *Glob. Biogeochem. Cycles*, 18,
759 <https://doi.org/10.1029/2004GB002227>, 2004.
- 760 Lamborg, C. H., Buesseler, K. O., Valdes, J., Bertrand, C. H., Bidigare, R., Manganini, S., Pike, S., Steinberg,
761 D., Trull, T., and Wilson, S.: The flux of bio- and lithogenic material associated with sinking particles in
762 the mesopelagic “twilight zone” of the northwest and North Central Pacific Ocean, *Deep Sea Res. Part II*
763 *Top. Stud. Oceanogr.*, 55, 1540–1563, <https://doi.org/10.1016/j.dsr2.2008.04.011>, 2008.
- 764 Letelier, R. M., Björkman, K. M., Church, M. J., Hamilton, D. S., Mahowald, N. M., Scanza, R. A.,
765 Schneider, N., White, A. E., and Karl, D. M.: Climate-driven oscillation of phosphorus and iron limitation
766 in the North Pacific Subtropical Gyre, *Proc. Natl. Acad. Sci.*, 116, 12720–12728,
767 <https://doi.org/10.1073/pnas.1900789116>, 2019.



- 768 Letscher, R. T. and Villareal, T. A.: Evaluation of the seasonal formation of subsurface negative
769 preformed nitrate anomalies in the subtropical North Pacific and North Atlantic, *Biogeosciences*, 15,
770 6461–6480, <https://doi.org/10.5194/bg-15-6461-2018>, 2018.
- 771 Liang, Z., Letscher, R. T., and Knapp, A. N.: Global patterns of surface ocean dissolved organic matter
772 stoichiometry, *Global Biogeochemical Cycles*, 37(12), e2023GB007788,
773 <https://doi.org/10.1029/2023GB007788>, 2023.
- 774 Ling, S. C. and Alldredge, A. L.: Does the marine copepod *Calanus pacificus* consume transparent
775 exopolymer particles (TEP)?, *J. Plankton Res.*, 25, 507–515, <https://doi.org/10.1093/plankt/25.5.507>,
776 2003.
- 777 Long, J., Fassbender, A., and Estapa, M.: Depth-Resolved Net Primary Production in the Northeast Pacific
778 Ocean: A Comparison of Satellite and Profiling Float Estimates in the Context of Two Marine Heatwaves,
779 *Geophys. Res. Lett.*, 48, <https://doi.org/10.1029/2021GL093462>, 2021.
- 780 Longhurst, A., Sathyendranath, S., Platt, T., and Caverhill, C.: An estimate of global primary production in
781 the ocean from satellite radiometer data, *J. Plankton Res.*, 17, 1245–1271,
782 <https://doi.org/10.1093/plankt/17.6.1245>, 1995.
- 783 Mari, X., Beauvais, S., Lemée, R., and Pedrotti, M. L.: Non-Redfield C:N ratio of transparent exopolymeric
784 particles in the northwestern Mediterranean Sea, *Limnol. Oceanogr.*, 46, 1831–1836,
785 <https://doi.org/10.4319/lo.2001.46.7.1831>, 2001.
- 786 Mari, X., Rochelle-Newall, E., Torrétion, J.-P., Pringault, O., Jouon, A., and Migon, C.: Water residence
787 time: A regulatory factor of the DOM to POM transfer efficiency, *Limnol. Oceanogr.*, 52, 808–819,
788 <https://doi.org/10.4319/lo.2007.52.2.0808>, 2007.
- 789 Mari, X., Passow, U., Migon, C., Burd, A. B., and Legendre, L.: Transparent exopolymer particles: Effects
790 on carbon cycling in the ocean, *Prog. Oceanogr.*, 151, 13–37,
791 <https://doi.org/10.1016/j.pocean.2016.11.002>, 2017.
- 792 McCarthy, M., Hedges, J., and Benner, R.: Major biochemical composition of dissolved high molecular
793 weight organic matter in seawater, *Mar. Chem.*, 55, 281–297, [https://doi.org/10.1016/S0304-
794 4203\(96\)00041-2](https://doi.org/10.1016/S0304-4203(96)00041-2), 1996.
- 795 Meers, E., Laing, G. D., Unamuno, V. G., Lesage, E., Tack, F. M. G., and Verloo, M. G.: Water Extractability
796 of Trace Metals from Soils: Some Pitfalls, *Water. Air. Soil Pollut.*, 176, 21–35,
797 <https://doi.org/10.1007/s11270-005-9070-1>, 2006.
- 798 Michaels, A. F., Bates, N. R., Buesseler, K. O., Carlson, C. A., and Knap, A. H.: Carbon-cycle imbalances in
799 the Sargasso Sea, *Nature*, 372, 537–540, <https://doi.org/10.1038/372537a0>, 1994.
- 800 Nagata, T., Yamada, Y., and Fukuda, H.: Transparent Exopolymer Particles in Deep Oceans: Synthesis and
801 Future Challenges, *Gels*, 7, 75, <https://doi.org/10.3390/gels7030075>, 2021.
- 802 Nosaka, Y., Yamashita, Y., and Suzuki, K.: Dynamics and Origin of Transparent Exopolymer Particles in the
803 Oyashio Region of the Western Subarctic Pacific during the Spring Diatom Bloom, *Front. Mar. Sci.*, 4,
804 2017.



- 805 Ortega-Retuerta, E., Passow, U., Duarte, C. M., and Reche, I.: Effects of ultraviolet B radiation on (not so)
806 transparent exopolymer particles, *Biogeosciences*, 6, 3071–3080, [https://doi.org/10.5194/bg-6-3071-](https://doi.org/10.5194/bg-6-3071-2009)
807 2009, 2009a.
- 808 Ortega-Retuerta, E., Reche, I., Pulido-Villena, E., Agustí, S., and Duarte, C. M.: Uncoupled distributions of
809 transparent exopolymer particles (TEP) and dissolved carbohydrates in the Southern Ocean, *Mar. Chem.*,
810 115, 59–65, <https://doi.org/10.1016/j.marchem.2009.06.004>, 2009b.
- 811 Ortega-Retuerta, E., Mazuecos, I. P., Reche, I., Gasol, J. M., Álvarez-Salgado, X. A., Álvarez, M., Montero,
812 M. F., and Arístegui, J.: Transparent exopolymer particle (TEP) distribution and in situ prokaryotic
813 generation across the deep Mediterranean Sea and nearby North East Atlantic Ocean, *Prog. Oceanogr.*,
814 173, 180–191, <https://doi.org/10.1016/j.pocean.2019.03.002>, 2019.
- 815 Pakulski, J. D. and Benner, R.: Abundance and distribution of carbohydrates in the ocean, *Limnol.*
816 *Oceanogr.*, 39, 930–940, <https://doi.org/10.4319/lo.1994.39.4.0930>, 1994.
- 817 Passow, U.: Formation of transparent exopolymer particles, TEP, from dissolved precursor material,
818 *Mar. Ecol. Prog. Ser.*, 192, 1–11, <https://doi.org/10.3354/meps192001>, 2000.
- 819 Passow, U.: Production of transparent exopolymer particles (TEP) by phyto- and bacterioplankton, *Mar.*
820 *Ecol. Prog. Ser.*, 236, 1–12, <https://doi.org/10.3354/meps236001>, 2002a.
- 821 Passow, U.: Transparent exopolymer particles (TEP) in aquatic environments, *Prog. Oceanogr.*, 55, 287–
822 333, [https://doi.org/10.1016/S0079-6611\(02\)00138-6](https://doi.org/10.1016/S0079-6611(02)00138-6), 2002b.
- 823 Passow, U., Alldredge, A. L., and Logan, B. E.: The role of particulate carbohydrate exudates in the
824 flocculation of diatom blooms, *Deep Sea Res. Part Oceanogr. Res. Pap.*, 41, 335–357,
825 [https://doi.org/10.1016/0967-0637\(94\)90007-8](https://doi.org/10.1016/0967-0637(94)90007-8), 1994.
- 826 Pilskaln, C. H., Villareal, T. A., Dennett, M., Darkangelo-Wood, C., and Meadows, G.: High concentrations
827 of marine snow and diatom algal mats in the North Pacific Subtropical Gyre: Implications for carbon and
828 nitrogen cycles in the oligotrophic ocean, *Deep Sea Res. Part Oceanogr. Res. Pap.*, 52, 2315–2332,
829 <https://doi.org/10.1016/j.dsr.2005.08.004>, 2005.
- 830 van Pinxteren, M., Robinson, T.-B., Zeppenfeld, S., Gong, X., Bahlmann, E., Fomba, K. W., Triesch, N.,
831 Stratmann, F., Wurl, O., Engel, A., Wex, H., and Herrmann, H.: High number concentrations of
832 transparent exopolymer particles in ambient aerosol particles and cloud water – a case study at the
833 tropical Atlantic Ocean, *Atmospheric Chem. Phys.*, 22, 5725–5742, [https://doi.org/10.5194/acp-22-](https://doi.org/10.5194/acp-22-5725-2022)
834 5725-2022, 2022.
- 835 Prairie, J. C., Montgomery, Q. W., Proctor, K. W., and Ghiorso, K. S.: Effects of Phytoplankton Growth
836 Phase on Settling Properties of Marine Aggregates, *J. Mar. Sci. Eng.*, 7, 265,
837 <https://doi.org/10.3390/jmse7080265>, 2019.
- 838 Quay, P., Emerson, S., and Palevsky, H.: Regional Pattern of the Ocean’s Biological Pump Based on
839 Geochemical Observations, *Geophys. Res. Lett.*, 47, e2020GL088098,
840 <https://doi.org/10.1029/2020GL088098>, 2020.



- 841 Rabouille, S., Cabral, G. S., and Pedrotti, M. L.: Towards a carbon budget of the diazotrophic
842 cyanobacterium *Crocospaera*: effect of irradiance, *Mar. Ecol. Prog. Ser.*, 570, 29–40,
843 <https://doi.org/10.3354/meps12087>, 2017.
- 844 Radić, T., Ivančić, I., Fuks, D., and Radić, J.: Marine bacterioplankton production of polysaccharidic and
845 proteinaceous particles under different nutrient regimes, *FEMS Microbiol. Ecol.*, 58, 333–342,
846 <https://doi.org/10.1111/j.1574-6941.2006.00176.x>, 2006.
- 847 Reintjes, G., Fuchs, B. M., Amann, R., and Arnosti, C.: Extensive Microbial Processing of Polysaccharides
848 in the South Pacific Gyre via Selfish Uptake and Extracellular Hydrolysis, *Front. Microbiol.*, 11, 2020.
- 849 Reygondeau, G., Longhurst, A., Martinez, E., Beaugrand, G., Antoine, D., and Maury, O.: Dynamic
850 biogeochemical provinces in the global ocean, *Glob. Biogeochem. Cycles*, 27, 1046–1058,
851 <https://doi.org/10.1002/gbc.20089>, 2013.
- 852 Rochelle-Newall, E. J., Mari, X., and Pringault, O.: Sticking properties of transparent exopolymeric
853 particles (TEP) during aging and biodegradation, *J. Plankton Res.*, 32, 1433–1442,
854 <https://doi.org/10.1093/plankt/fbq060>, 2010.
- 855 Roshan, S. and DeVries, T.: Efficient dissolved organic carbon production and export in the oligotrophic
856 ocean, *Nat. Commun.*, 8, 2036, <https://doi.org/10.1038/s41467-017-02227-3>, 2017.
- 857 Sambrotto, R. N., Savidge, G., Robinson, C., Boyd, P., Takahashi, T., Karl, D. M., Langdon, C., Chipman, D.,
858 Marra, J., and Codispoti, L.: Elevated consumption of carbon relative to nitrogen in the surface ocean,
859 *Nature*, 363, 248–250, <https://doi.org/10.1038/363248a0>, 1993.
- 860 Smith, D. C., Simon, M., Alldredge, A. L., and Azam, F.: Intense hydrolytic enzyme activity on marine
861 aggregates and implications for rapid particle dissolution, *Nature*, 359, 139–142,
862 <https://doi.org/10.1038/359139a0>, 1992.
- 863 Smyth, A. J., and Letscher, R. T.: Spatial and temporal occurrence of preformed nitrate anomalies in the
864 subtropical North Pacific and North Atlantic oceans, *Marine Chemistry*, 252, 104248,
865 <https://doi.org/10.5194/bg-15-6461-2018>, 2023.
- 866 Sun, C.-C., Sperling, M., and Engel, A.: Effect of wind speed on the size distribution of gel particles in the
867 sea surface microlayer: insights from a wind–wave channel experiment, *Biogeosciences*, 15, 3577–3589,
868 <https://doi.org/10.5194/bg-15-3577-2018>, 2018.
- 869 Teng, Y.-C., Primeau, F. W., Moore, J. K., Lomas, M. W., and Martiny, A. C.: Global-scale variations of the
870 ratios of carbon to phosphorus in exported marine organic matter, *Nat. Geosci.*, 7, 895–898,
871 <https://doi.org/10.1038/ngeo2303>, 2014.
- 872 Thompson, A. W., van den Engh, G., Ahlgren, N. A., Kouba, K., Ward, S., Wilson, S. T., and Karl, D. M.:
873 Dynamics of *Prochlorococcus* Diversity and Photoacclimation During Short-Term Shifts in Water Column
874 Stratification at Station ALOHA, *Front. Mar. Sci.*, 5, 2018.
- 875 Thornton, D. C. O.: Coomassie Stainable Particles (CSP): Protein Containing Exopolymer Particles in the
876 Ocean, *Front. Mar. Sci.*, 5, 2018.



- 877 Toggweiler, J. R.: Carbon overconsumption, *Nature*, 363, 210–211, <https://doi.org/10.1038/363210a0>,
878 1993.
- 879 Villareal, T. A., Pilskaln, C. H., Montoya, J. P., and Dennett, M.: Upward nitrate transport by
880 phytoplankton in oceanic waters: balancing nutrient budgets in oligotrophic seas, *PeerJ*, 2, e302,
881 <https://doi.org/10.7717/peerj.302>, 2014.
- 882 Westberry, T. K., Silsbe, G. M., and Behrenfeld, M. J.: Gross and net primary production in the global
883 ocean: An ocean color remote sensing perspective, *Earth-Sci. Rev.*, 237, 104322,
884 <https://doi.org/10.1016/j.earscirev.2023.104322>, 2023.
- 885 Williams, P. J. le B., Quay, P. D., Westberry, T. K., and Behrenfeld, M. J.: The Oligotrophic Ocean Is
886 Autotrophic, *Annu. Rev. Mar. Sci.*, 5, 535–549, <https://doi.org/10.1146/annurev-marine-121211-172335>,
887 2013.
- 888 Wurl, O., Wurl, E., Miller, L., Johnson, K., and Vagle, S.: Formation and global distribution of sea-surface
889 microlayers, *Biogeosciences*, 8, 121–135, <https://doi.org/10.5194/bg-8-121-2011>, 2011a.
- 890 Wurl, O., Miller, L., and Vagle, S.: Production and fate of transparent exopolymer particles in the ocean,
891 *J. Geophys. Res. Oceans*, 116, <https://doi.org/10.1029/2011JC007342>, 2011b.
- 892 Zamanillo, M., Ortega-Retuerta, E., Nunes, S., Estrada, M., Sala, M. M., Royer, S.-J., López-Sandoval, D.
893 C., Emelianov, M., Vaqué, D., Marrasé, C., and Simó, R.: Distribution of transparent exopolymer particles
894 (TEP) in distinct regions of the Southern Ocean, *Sci. Total Environ.*, 691, 736–748,
895 <https://doi.org/10.1016/j.scitotenv.2019.06.524>, 2019.
- 896 Zamanillo, M., Ortega-Retuerta, E., Cisternas-Novoa, C., Marrasé, C., Pelejero, C., Pascual, J., Gasol, J. M.,
897 Engel, A., and Simó, R.: Uncoupled seasonal variability of transparent exopolymer and Coomassie
898 stainable particles in coastal Mediterranean waters: Insights into sources and driving mechanisms, *Elem.
899 Sci. Anthr.*, 9, 00165, <https://doi.org/10.1525/elementa.2020.00165>, 2021.
- 900 Zäncker, B., Bracher, A., Röttgers, R., and Engel, A.: Variations of the Organic Matter Composition in the
901 Sea Surface Microlayer: A Comparison between Open Ocean, Coastal, and Upwelling Sites Off the
902 Peruvian Coast, *Front. Microbiol.*, 8, 2017.
- 903
- 904